Accepted Manuscript

Hydrophobicity-oriented drug design (HODD) of new human 4-hydroxyphenylpyruvate dioxygenase inhibitors

Ferdinand Ndikuryayo, Wei-Ming Kang, Feng-Xu Wu, Wen-Chao Yang, Guang-Fu Yang

PII: S0223-5234(19)30042-X

DOI: https://doi.org/10.1016/j.ejmech.2019.01.032

Reference: EJMECH 11039

To appear in: *European Journal of Medicinal Chemistry*

Received Date: 18 November 2018

Revised Date: 13 January 2019

Accepted Date: 13 January 2019

Please cite this article as: F. Ndikuryayo, W.-M. Kang, F.-X. Wu, W.-C. Yang, G.-F. Yang, Hydrophobicity-oriented drug design (HODD) of new human 4-hydroxyphenylpyruvate dioxygenase inhibitors, *European Journal of Medicinal Chemistry* (2019), doi: https://doi.org/10.1016/j.ejmech.2019.01.032.

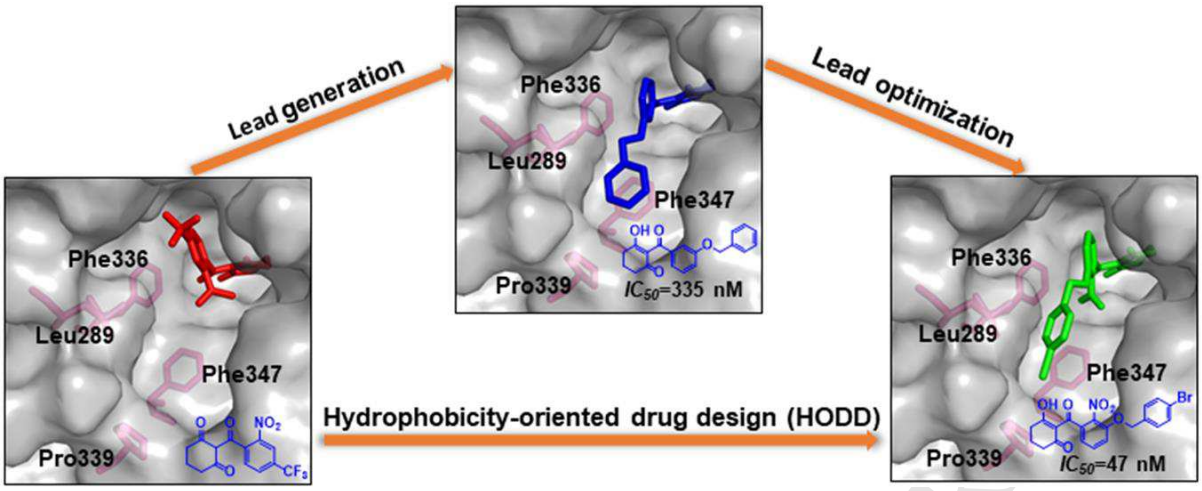

Hydrophobicity-Oriented Drug Design (HODD) of New Human 4-Hydroxyphenylpyruvate dioxygenase Inhibitors

Ferdinand Ndikuryayo[a], Wei-Ming Kang[a], Feng-Xu Wu[a], Wen-Chao Yang*[a], Guang-Fu Yang*[a,b]

[a]Key Laboratory of Pesticide & Chemical Biology of Ministry of Education, International Joint Research Center for Intelligent Biosensor Technology and Health, and Chemical Biology Center, College of Chemistry, Central China Normal University, Wuhan 430079, P.R. China;

[b]Collaborative Innovation Center of Chemical Science and Engineering, Tianjin 30071, P.R. China.

*Wen-Chao Yang, e-mail: tomyang@mail.ccnu.edu.cn; Tel: +86-27-67867706; Fax: +86-27-7867141; Guang-Fu Yang, e-mail: gfyang@mail.ccnu.edu.cn; Tel: +86-27-67867800; Fax: +86-27-67867141.

Abstract

Involved in the tyrosine degradation pathway, 4-hydroxyphenylpyruvate dioxygenase (HPPD) is an important target for treating type I tyrosinemia. To discover novel HPPD inhibitors, we proposed a hydrophobicity-oriented drug design (HODD) strategy based on the interactions between HPPD and the commercial drug NTBC. Most of the new compounds showed improved activity, compound **d23** being the most active candidate (IC_{50} = 0.047 μM) with about 2-fold more potent than NTBC (IC_{50} = 0.085 μM). Therefore, compound **d23** is a potential drug candidate to treat type I tyrosinemia.

Keywords: Hydrophobicity-oriented drug design (HODD), 4-hydroxyphenylpyruvate dioxygenase, inhibitors, type I tyrosinemia, alkaptonuria, hawkinisinuria.

1. Introduction

Existing in all aerobic organisms except some gram-positive bacteria [1,2], 4-hydroxyphenylpyruvate dioxygenase (HPPD, EC:1.13.11.27) converts 4-hydroxyphenylpyruvic acid (HPPA) into homogentisic acid (HGA) in the tyrosine breakdown pathway [3]. As shown in Scheme 1, four of the five enzymes involved in this crucial pathway are associated with human diseases [4].

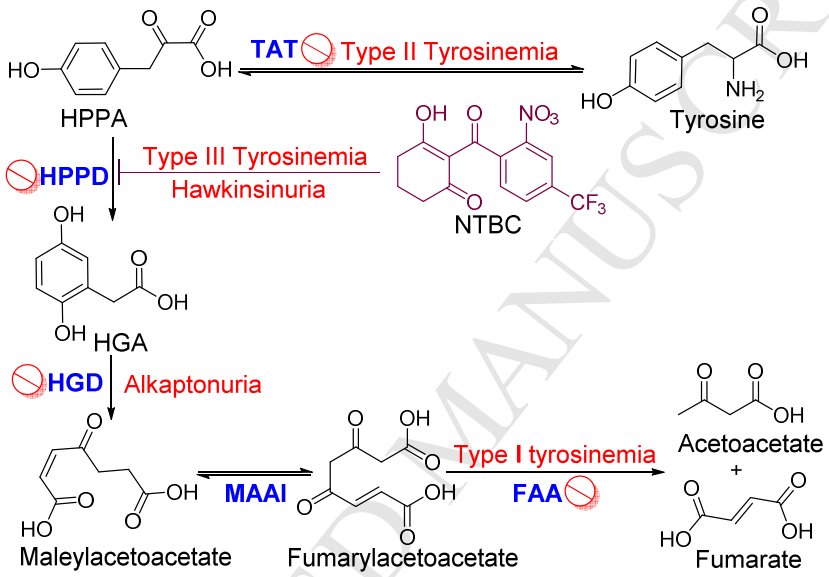

Scheme 1. Simplified tyrosine breakdown pathway and associated diseases (red). Enzymes (blue) and substrates are abbreviated as following: TAT, tyrosine aminotransferase; HPPA, hydroxyphenylpyruvic acid; HPPD, hydroxyphenylpyruvate dioxygenase; HGA, homogentesic acid; HGD, homogentisate 1,2-dioxygenase; MAA, maleylacetoacetate; MAAI, maleylacetoacetate isomerase. The red "stop" signs indicate the enzyme failure.

The deficiency of tyrosine aminotransferase results in type II tyrosinemia whose symptoms comprise mental retardation, photophobia, keratitis, painful corneal eruptions, and painful palmoplantar hyperkeratosis [5]. The weakness of HPPD could cause either hawkinsinuria or type III tyrosinemia [6]. Characterized by failure to grow, permanent metabolic acidosis, and fine and sparse hair, hawkinsinuria evolves from an autosomal dominant N241S mutation that produces a variant

enzyme. Instead of the native homogentisic acid (HGA), the variant HPPD produces an active quinolacetic acid that reacts with cellular thiols to generate a two-electron oxidized form of hawkinsin [7]. Type III tyrosinemia, the rarest deficiency of tyrosine degradation pathway, is due to pathogenic mutations in HPPD gene whose dysfunction results in mental retardation or neurological symptoms [8]. A defective homogentisate 1,2-dioxygenase (HGD) leads to alkaptonuria, a disease associated with an increased level of plasma HGA whose accumulation and polymerization in cartilage results in osteoarthropathy [9]. Type I tyrosinemia, the most severe deficiency of the tyrosine breakdown pathway, is due to the failure of fumarylacetoacetase (FAA) that induces the accumulation of fumarylacetoacetate and maleylacetoacetate (Scheme 1). These two metabolites can then be converted into succinylacetone, the cause of liver failure, painful neurologic crises, rickets, and hepatocarcinoma [10]. Fumarylacetoacetate and succinylacetone are the most harmful metabolites. For example, besides being mutagenic, fumarylacetoacetate could induce apoptosis, and prevent DNA repair, whereas succinylacetone prevents the heme synthesis [4].

Initially staked on the liver transplantation, the treatment of type I tyrosinemia is currently based on NTBC, a synthetic compound that inhibits human HPPD [11,12]. Blocking the pathway at this step made HPPD a favorite target to treat associated diseases because it prevents the formation of the aforesaid harmful metabolites. Interestingly, this blockage did not induce the liver damage [6]. Besides the treatment of type I tyrosinemia, NTBC could also alleviate the symptoms of alkaptonuria and hawkinisinuria [7,13]. However, recent studies have reported NTBC drawbacks. For example, NTBC could not induce a response in one of ten treated children, whereas another developed hepatic dysplasia associated with poor quality of life [14]. Next to this finding, recent studies have shown that NTBC might cause a significant decrease in intellectual quotient (IQ) in patients and corneal lesions in rats [15,16]. At present, it is uncertain if this unique medication will be appropriate to prevent

problems for a long-term period of time, therefore, suggesting the need for the discovery and development of new drugs.

As known to all, computer-aided drug design (CADD) is classified into ligand-based and protein structure-based design, and has become an essential part of the drug discovery pipeline [17]. Whereas ligand-based design consists in the building of 3D pharmacophore models based on existing compounds, structure-based drug design involves the design of small molecules based on the shape and chemical features of a known three-dimensional structure of a target enzyme [17]. We performed the molecular docking of NTBC into human HPPD active pocket, and found an empty hydrophobic region surrounded by Phe347 residue at the active site (Figure 1B). Thus, we hypothesized that a π-π stacking interaction between Phe347 and inhibitor may increase the hydrophobic interaction with HPPD pocket, and thus improves the inhibitory activity. Therefore, we proposed a hydrophobicity-oriented drug design (HODD) strategy to design new HPPD inhibitors. Guided by this rationale, we introduced a benzyloxy substituent at the meta position of the benzene ring of NTBC, and prepared a series of new 2-(3-(benzyloxy)benzoyl)-3-hydroxycyclohex-2-en-1-one analogs as novel human HPPD inhibitors.

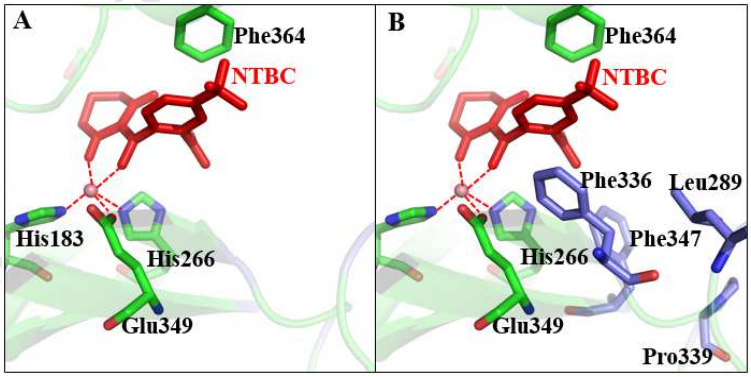

Figure 1. Identification of the free region for the optimal filling of the human HPPD active site. While (A) shows the binding mode of NTBC (red), (B) depicts the empty region surrounded by hydrophobic residues (blue).

As expected, the inhibitory activity of the tested compounds was in nanomolar range against recombinant human HPPD. A number of compounds exhibited improved activity, and compound **d23** (IC_{50} = 0.047 μM), the most active candidate, showed about 2-fold more potency than NTBC (IC_{50} = 0.085 μM).

2. Results and discussion

2.1. Molecular modelling and lead compound design

Molecular modeling is used to simulate the binding modes of small molecules in a target enzyme. Thus, in this study, NTBC was docked into the human HPPD active site to explore its binding mode (Figure 2). Because there was no available NTBC-bound human HPPD crystal structure, the HPPD crystal structure derived from rat HPPD (PDB ID: 1SQI) was selected as template to model human HPPD three-dimensional structure using human HPPD sequence (NCBI GI: 258588704). By analyzing the binding mode, we located an empty region in the human HPPD active site.

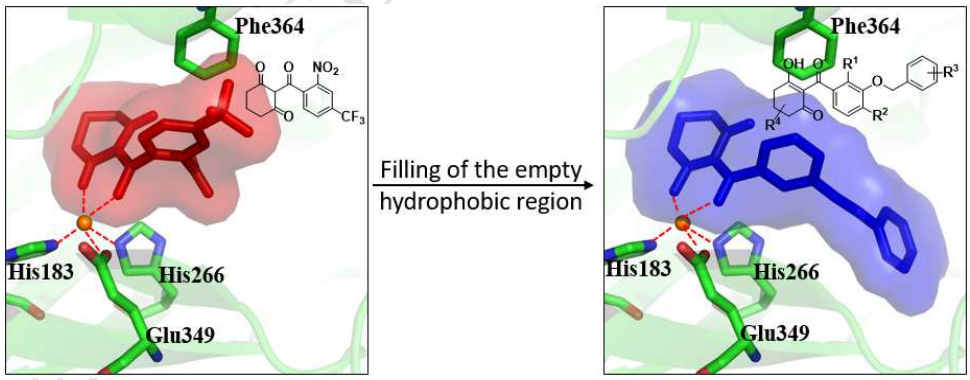

Figure 2. Design strategy of the 2-(3-(benzyloxy)benzoyl)-3-hydroxycyclohex-2-en-1-one analogs as new human HPPD inhibitors.

Given that HPPD is competitively inhibited, we hypothesized that the optimal filling of the active site may increase the enzyme inhibition. It was then crucial to characterize the chemical properties of

the empty region. To this end, the *Arabidopsis thaliana* HPPD crystal in complex with NTBC (PDB ID: 5CTO) was superimposed with human HPPD. As result, important residues including Leu287, Phe336, Pro339, and Phe347 were located in the empty region. Based on the hydrophobic character of these residues, we concluded that the empty region was hydrophobic (Figure 1B). We further hypothesized that a π-π stacking interaction between Phe347 and inhibitor may increase the inhibitory activity. We then added a virtual hydrophobic fragment to NTBC-derived scaffold and docked the resultant structure into human HPPD active site to generate the structure of the title compound.

The binding mode of the lead compound in the active site showed beneficial features for further optimization. Beside the Fe^{2+}-chelation found in all triketone-containing HPPD inhibitors (Figure 3A) [18], π-π stacking interaction was formed between the benzene ring of the newly added fragment and Phe347 as expected (Figure 3B). The displacement of the middle benzene ring in favor of face-to-face (sandwich) π-π interaction with both Phe336 and Phe364 was also observed (Figure 3C). For the sake of structure optimization, a series of analogs were synthesized and tested against recombinant human HPPD.

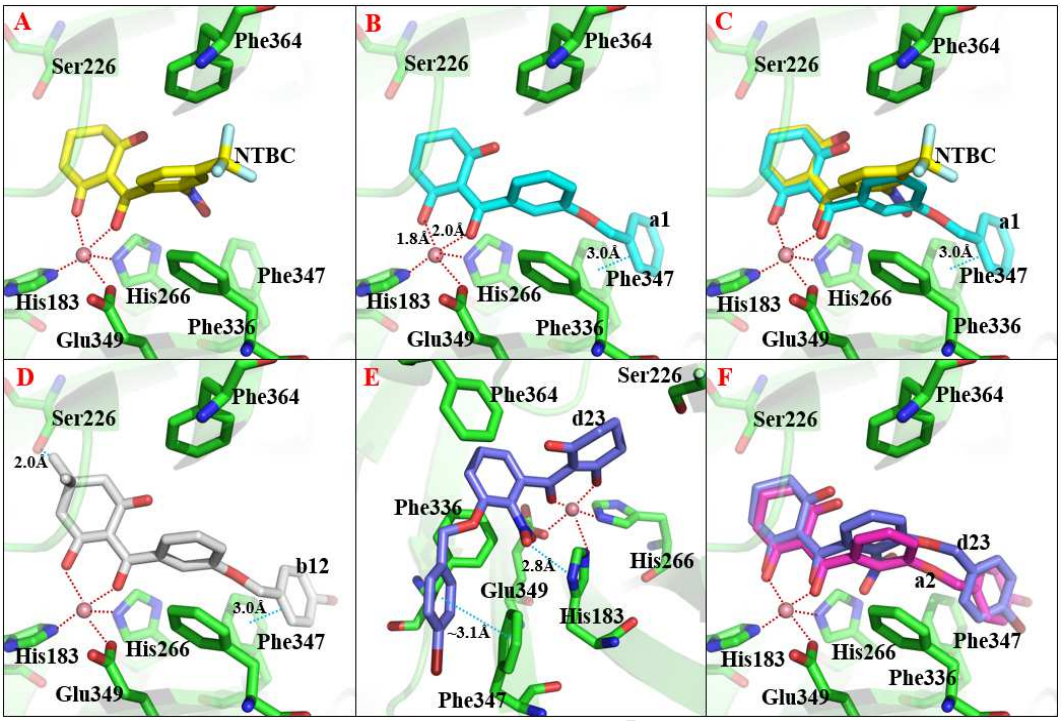

Figure 3. Simulated binding modes of selected compounds in human HPPD active site. Red and blue-dashed lines represent the Fe^{2+}-chelating and other interactions, respectively. Fe^{2+} is depicted by pink sphere, and key residues in green. Beside Fe^{2+}-chelating and sandwich interactions of bound NTBC (A), compound **a1** (B) showed additional π-π interaction with Phe347 along with displacement of the middle benzene ring in favor of face-to-face π-π interaction with both Phe336 and Phe364 (C). The decreased activity of compound **b12** was due to steric hindrance (D) while the high potency of compound **d23** was attributed to hydrogen bond (E) that adjusted its binding mode (F).

2.2. Chemistry

The preparation of the title compound **6** was shown in Scheme 2. The synthesis followed a six-step synthetic route starting from the commercially available 3-hydroxybenzoic acid. 3-hydroxybenzoic acid was esterified to afford compound **1**, which was then treated with *p*-bromobenzyl bromide in the presence of anhydrous potassium carbonate (K_2CO_3) in *N*,*N*-dimethylformamide (DMF) to produce the compound **2**. This product was hydrolyzed using sodium hydroxide (NaOH) in

methanol to yield the product **3** that reacted with oxalyl chloride in the presence of DMF as catalyst to speed up the reaction that yielded compound **4**. Intermediates **3** (**3a-k**) were synthesized and characterized as shown in Supporting Information. The reaction was followed by esterification with cyclohexane-1,3-dione using triethylamine as a base in dichloromethane to get the key enol ester **5**. Finally, acetone cyanohydrin catalyzed Fries-type rearrangement of enolesther **5** was performed by using triethylamine in anhydrous acetonitrile at room temperature to afford tittle compound **6** in good yield (61-69%). Intermediates **5** (**5a-p**) were synthesized and characterized as shown in Supporting Information. All the structures of target compounds were characterized by ^{1}H NMR and high-resolution mass spectral data whereas ^{13}C NMR was only applied to target compounds.

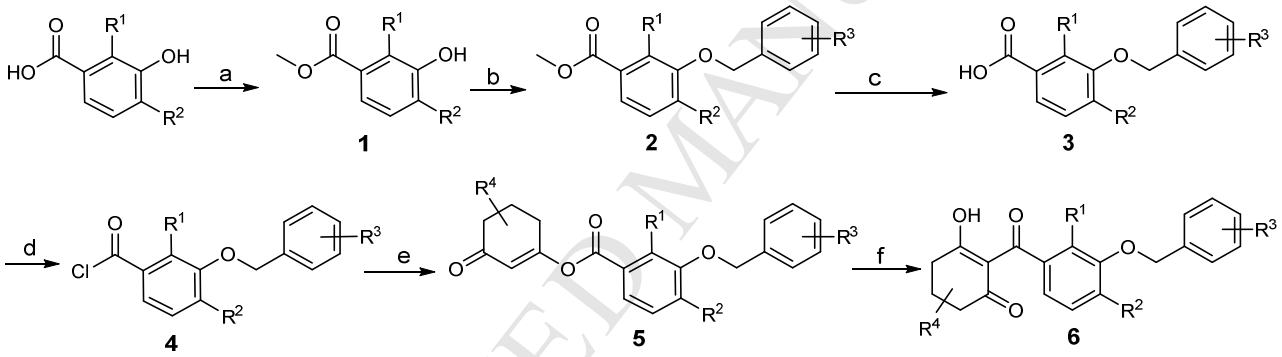

Reagents and conditions: (a) $SOCl_2$, CH_3OH, 60 °C; (b) K_2CO_3, DMF, $C_7H_6Br_2$, 80 °C; (c) NaOH, CH_3OH: H_2O (1:1), reflux; (d) Oxalyl chloride, CH_2Cl_2, -5°C, DMF; (e) Substituted1,3-cyclohexanedione, Et_3N, CH_2Cl_2, -5 °C; (f) Acetone cyanohydrin, Et_3N, CH_3CN, rt.

Scheme 2. Synthetic route of the title compound

In the final step of the rearrangement reaction, the reaction system was simple and complete. The target compound was extracted using column chromatography. However, the reaction yield was low because the target compound not only had a certain water solubility but also was adsorbed on the column.

2.3. Enzyme inhibition and structure-activity relationship (SAR) study

Using the coupled enzyme reaction, the inhibitory activity of synthesized compounds was evaluated, using NTBC as the positive control. For this purpose, the recombinant human HPPD was purified using Ni-NTA column chromatography. The enzyme purity was validated by sodium dodecyl sulfate-polyacrylamide gel electrophoresis (SDS-PAGE) (Figure 4), and was estimated to be 92% using ImageJ software (ImageJ 1.52a, Bethesda, MD, USA).

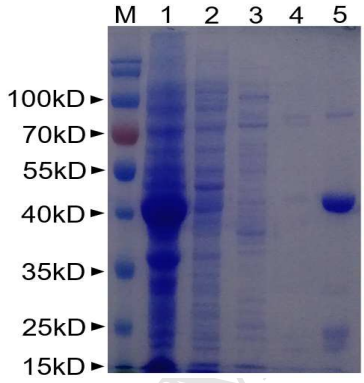

Figure 4. Validation of the over-expression of recombinant human HPPD by SDS-PAGE. M, marker; lane 1, cell-free supernatant, lanes 2 to 5, elution with 0, 10, 30 and 250 mM imidazole, respectively. Lane 5 represents the purified enzyme.

The structure-activity relationship (SAR) of synthesized analogs was analyzed. Based on the position and the type of substituents on the title compound **6**, all the compounds were divided into 4 groups for the sake of clarity. With $R^1 = R^2 = R^4 = H$, the introduction of electron withdrawing (F, Cl and Br) groups at the 4-position of the aryloxyphenyl ring considerably increased the inhibitory activities. For example, Br, the most active group (**a2**, IC_{50} = 0.091 μM), showed a 4-fold increase in activity compared with unsubstituted parent **a1** (IC_{50} = 0.335 μM). However, the 4-Br-induced improvement in activity was compromised by introducing methyl substituents on 5-position (R^4) of the benzene ring of triketone moiety. We observed for example, in comparison with compound **a2**, at least

a 2-fold decrease in inhibitory activity in compounds **b11**, **b12** and **b13**. Compared with their respective counterparts **c19**, **d29** and **d31**, a similar trend was also observed in compounds **c20**, **d30** and **d32**, suggesting the presence of a steric hindrance that might significantly reduce the potency [19,20]. Methylation of the middle benzene ring (R^1 = CH_3) of the halogenated compounds significantly decreased the inhibitory activity (**c14-c20**). Despite the disadvantageous effect of methylation at R^1, the chlorination of the same benzene ring (R^2 = Cl) (**c22** and **c23**) resulted in improved activity, therefore, suggesting that introducing electron withdrawing groups at R^2 may afford more potent human HPPD inhibitors. Interestingly, nitration of the middle benzene ring (R^1 = NO_2) considerably increased the inhibitory activity. For example, seven compounds (**d23**, **d24**, **d26**, **d27**, **d29**, **d31** and **d33**) exhibited similar to higher inhibitory activity compared with NTBC, compound **d23** (IC_{50} = 0.047 µM) being the most active, about 2-fold higher than NTBC (IC_{50} = 0.085 µM) (Table 1).

Table 1. Chemical structures of new compounds and their biological activity against recombinant human HPPD.

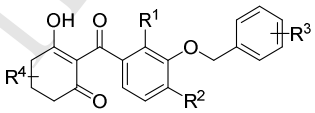

compound	R^1	R^2	R^3	R^4	IC_{50} (µM)
NTBC		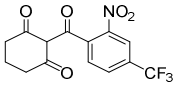			0.085±0.005
a1	H	H	H	H	0.335±0.016
a2	H	H	4-Br	H	0.091±0.003
a3	H	H	4-Cl	H	0.217±0.019
a4	H	H	4-F	H	0.264±0.013
a5	H	H	3-F	H	0.274±0.020
a6	H	H	4-CH_3	H	0.266±0.016
a7	H	H	2,4-diCl	H	0.143±0.007
a8	H	H	2-F	H	0.422±0.019
a9	H	H	2-F-4-Br	H	0.121±0.005
a10	H	H	2-F-4-Cl	H	0.147±0.006

b11	H	H	2-F-4-Br	5-CH_3	0.200±0.009
b12	H	H	4-Br	5,5-diCH_3	0.558±0.049
b13	H	H	4-Br	5-CH_3	0.176±0.009
c14	CH_3	H	4-Br	H	0.274±0.015
c15	CH_3	H	4-Cl	H	0.266±0.005
c16	CH_3	H	4-CH_3	H	0.374±0.021
c17	CH_3	H	4-F	H	0.302±0.003
c18	CH_3	H	3-Br	H	0.280±0.013
c19	CH_3	H	2-F-4-Cl	H	0.257±0.010
c20	CH_3	H	2-F-4-Cl	5-CH_3	0.447±0.022
c21	CH_3	Cl	H	H	0.128±0.005
c22	CH_3	Cl	4-F	H	0.102±0.006
d23	NO_2	H	4-Br	H	0.047±0.004
d24	NO_2	H	4-CH_3	H	0.070±0.004
d25	NO_2	H	4-F	H	0.128±0.005
d26	NO_2	H	4-$CH(CH_3)_2$	H	0.070±0.003
d27	NO_2	H	3,5-diCH_3	H	0.068±0.005
d28	NO_2	H	4-CH_3	5-CH_3	0.168±0.006
d29	NO_2	H	2-F-4-Br	H	0.068±0.003
d30	NO_2	H	2-F-4-Br	5-CH_3	0.105±0.004
d31	NO_2	H	2,4-diCl	H	0.063±0.005
d32	NO_2	H	2,4-diCl	5-CH_3	0.106±0.007
d33	NO_2	H	2,4-diF	H	0.095±0.005

To understand the structure-activity relationship (SAR) at the atomic level, selected compounds (**a1**, **a2**, **b12**, and **d23**) and NTBC were docked into human HPPD active site, and their respective binding modes and affinities were generated accordingly. As depicted in Figure 3A, NTBC was bound in human HPPD active site by Fe^{2+}-chelation in which five-coordinate were made by residues (Glu349, His183, and His266) and 5' and 7' oxygens of NTBC. The former chelating interaction was consolidated by Phe364, which in combination with Phe336, sandwiches the NTBC phenyl ring [21]. The binding mode of the parent compound **a1** also showed a similar pattern (Figure 3B) with a reduced Fe^{2+}-chelation distance. In comparison with reported human HPPD inhibitors, for example, while compound **a1** was located at 2.0 Å and 1.8 Å of Fe^{2+} (Figure 3B), the distance between pyarazole-benzimidazolone hybrid and Fe^{2+} was 2.5 Å and 2.7 Å [22]. Moreover, this distance was reported to be 1.9 Å and 3.4 Å for pyrazolone-quinazolone hybrid [19]. Interestingly, superimposition of NTBC and **a1** (Figure 3C) confirmed the formation of π-π stacking interaction between the newly

added benzene ring of **a1** and Phe347. Also, a displacement of the middle benzene ring of **a1** in favor of face-to-face (sandwich) π-π interaction with both Phe336 and Phe364 was confirmed (Figure 3C). Altogether, the aforementioned interactions may significantly contribute to the stabilization of **a1** and analogs in human active site.

The presence of dimethyl group on the benzene ring of triketone moiety (**b12)** resulted in more than 5-fold decrease in activity due to steric hindrance with Ser226 (Figure 3D). On another hand, compared with **a1**, the remarkable activity of compound **a2** might come from the presence of Br group on the benzene ring that improved the interaction. This Br-induced activity was consolidated by the nitration of the middle benzene ring ($R^1 = NO_2$) that resulted in an additional hydrogen bond (N-H···O interaction) between His266 and -NO_2 group (Figure 3E). As shown by superimposition of **d23** and **a2** (Figure 3F), the resultant interaction stabilized **d23** by adjusting its binding mode. This assumption was corroborated by the binding energy of **d23** (-10.73 Kcal/mol) that has more contribution for the binding compared with others (Table 2).

Table 2. Binding free energy calculated for the compounds (Kcal/mol)

Cpd	H-bond[a]	Electrostatic[b]	VDW[c]	Conformation entropy[d]	Desolvation[e]	Binding free energy
a1	-0.01	-1.88	-9.29	1.79	2.13	-7.27
a2	-0.01	-1.77	-9.06	1.79	2.16	-6.89
b12	-0.01	-1.46	-9.29	1.79	2.22	-6.75
c14	-0.01	-1.85	-9.11	1.76	2.16	-7.06
d23	-0.02	-1.89	-10.73	2.08	2.88	-7.66
NTBC	-0.02	-1.64	-9.68	1.49	2.51	-7.34

[a]Hydrogen bonding term. [b]Electrostatic energies term. [c]van der Waals term. [d]conformation entropy contribution. [e]desolvation contribution

In the light of our findings, beside the great potential of 2-(3-(benzyloxy)benzoyl)-3-hydroxycyclohex-2-en-1-one analogs for the discovery of more potent human HPPD inhibitors, compound **d23**, with about 2-fold more potent than NTBC, could be used as potential drug for the treatment of type I tyrosinemia, alkaptonuria and hawkinsinuria. Using various electronic withdrawing

groups, much more optimization of the title compound **6**, particularly at R^2, may afford more potent human HPPD inhibitors.

3. Conclusion

In summary, a new strategy of HODD was developed for the structure-based design of HPPD inhibitors, and thus a series of 2-(3-(benzyloxy)benzoyl)-3-hydroxycyclohex-2-en-1-one analogs were synthesized and tested as human HPPD inhibitors. On the basis of the bioevaluation assay, most of the newly synthesized compounds exhibited significant human HPPD inhibitory activity and some compounds showed similar to higher efficiency in comparison with NTBC (IC_{50} = 0.085 μM). Moreover, compound **d23** was discovered to be the most active candidate (IC_{50} = 0.047 μM) with about 2-fold increase in activity. Threrfore, analogs of 2-(3-(benzyloxy)benzoyl)-3-hydroxycyclohex-2-en-1-one could serve as a novel lead scaffold for discovering new human HPPD inhibitors, while compound **d23** is a potential drug candidate to treat type I tyrosinemia, alkaptonuria, and hawkinsinuria.

4. Experimental section

4.1 Methods and synthesis

All chemical reagents were commercially available and treated with standard methods before use. ^{1}H NMR and ^{13}C NMR were recorded on Varian NMR 400 MHz and 600 MHz NMR (Varian, Palo Alto, CA), Bruker NMR 500 MHz NMR (Bruker, Madison, WI) with TMS as the internal standard, and deuterated chloroform ($CDCl_3$), deuterated-dimethyl sulfoxide (DMSO-d_6) as solvents. The following abbreviations are used to designate multiplicities: s=singlet, d=doublet, t=triplet, m=multiplet, dd=doublet of doublets, dt=doublet of triplets. Mass spectrometry (MS) and high resolution mass spectrometry (HRMS) data were obtained using DSQII GC-MS mass spectrometer (Thermo Fisher, Austin, TX) and 6224 TOF LC/MS Mass spectrometer (Agilent Technologies, Santa

Clara, CA). Melting points were taken on a Buchi B-545 without correction. Column chromatography silica gel (200-300 mesh) and TLC thin-layer chromatography silica gel plate were purchased from Qingdao Ocean Chemical Plant. The boiling range of petroleum ether was 60-90 °C.

4.1.1. General procedure for intermediate 1

3-Hydroxybenzoic acid (10 mmol) and anhydrous methanol (20 mL) were added to a 100 mL dry eggplant-shaped flask. With stirring, thionyl chloride (25 mmol) was added dropwise 5-12 h at 60 °C, and the reaction progress was tracked using TLC. After the reaction completion, excess thionyl chloride was removed under reduced pressure, and the system was slowly poured into 100 mL of ice water. The mixture was extracted with ethyl acetate (30 mL×3), the combined organic layer was dried over Na_2SO_4, concentrated under vaccum. The crude product **1** was used in the next step without further purification.

4.1.2. General procedure for intermediate 2

Compound **1** (10 mmol), anhydrous potassium carbonate (20 mmol, K_2CO_3) and DMF (20 mL) were added to a 100 mL-dry eggplant flask and stirred at room temperature for 30 min prior to addition of *p*-bromobenzyl bromide (12 mmol). The resulting mixture was maintained at 80 °C for 3-8 h, and the reaction course was monitored using TLC. Upon the reaction completion, the mixture was cooled to room temperature before the addition of 100 mL of water, and the system was extracted with ethyl acetate (30 mL×3). The organic phase was dried over anhydrous Na_2SO_4 and concentrated using rotary evaporator. The crude product **2** was used in the next step without further purification.

4.1.3. General procedure for intermediate 3

Compound **2** (10 mmol), NaOH (20 mmol), methanol (10 mL) and water (10 mL) were added to a 100 mL clean eggplant flask. The reaction mixture was heated at reflux for 1-2 h, and monitored by TLC. After the reaction was completed, methanol was removed from the system under reduced pressure

followed by the addition of 50 mL of water, and the mixture was washed with diethyl ether (20 mL×2). The aqueous phase was acidified to pH=1-2, the white solid was precipitated. The obtained solid was filtered and dried to give pure compounds **3**. The characterization of important intermediates (**3** and **5**) and the spectra of representative compounds were displayed in the Supporting Information (Figures S1-S7).

4.1.4. General procedure for intermediate 4

Compound **3** (5 mmol) and dichloromethane (10 mL) were added to 50 mL dry eggplant-shaped flask and stirred at 0 °C for 5 min. The redistilled oxalyl chloride (12.5 mmol) was added dropwise followed by the addition of a catalytic amount of DMF (3-5 drops). The mixture was then stirred for 3-5 h, and the progress of the reaction was monitored by TLC. After the completion of the reaction, the dichloromethane is removed under reduced pressure to obtain the acid chloride **4.**

4.1.5. General procedure for intermediate 5

Cyclohexanedione (6 mmol), dichloromethane (15 mL) and triethylamine (10 mmol) were added to a 100 mL eggplant-shaped flask, stirred for 10 min at 0°C. Subsequently, the intermediate **4** was dissolved in 15 mL of dry dichloromethane before addition to the above system. The reaction was carried out for 0.5-1 h and monitored by TLC. Upon the completion of the reaction, the reaction system was washed with water (20 mL), saturated sodium bicarbonate solution (20 mLx2), and brine (20 mL). The organic phase was then dried over anhydrous Na_2SO_4 and concentrated by rotary evaporation. The residue was purified via flash column chromatography to give **5**.

4.1.6. General procedure for target compounds

Compounds **5** (2 mmol), acetonitrile (20 mL), triethylamine (4 mmol) and acetone cyanohydrin (0.2 mmol) were added to a 100 mL eggplant-shaped flask, stirred for 20 h at room temperature, TLC was used to track the reaction progress until the complete disappearance of **5**. The system was then diluted

with aqueous HCl solution (30 mL, 1 M) and stirred for 5 min. The obtained solid was filtered, dried and then recrystallized in methanol to give title compounds **6** that were classified into four series (**a**, **b**, **c** and **d**).

4.1.7. 2-(3-(Benzyloxy)benzoyl)-3-hydroxycyclohex-2-en-1-one (a1)

Light yellow solid, Yield: 64%. m.p. 80.3-81.8 °C. ^{1}H NMR (600 MHz, $CDCl_3$) δ 7.43 (d, J=7.2 Hz, 2H), 7.39 (t, J=7.2 Hz, 2H), 7.35-7.28 (m, 2H), 7.15-7.07 (m, 3H), 5.07 (s, 2H), 2.78-2.69 (m, 2H), 2.53-2.44 (m, 2H), 2.06 (dt, J=13.2, 6.6 Hz, 2H). ^{13}C NMR (150 MHz, $CDCl_3$) δ 198.77, 195.86, 194.19, 158.24, 139.49, 136.60, 128.78, 128.57, 128.03, 127.58, 120.97, 118.48, 114.16, 113.34, 70.13, 38.01, 32.25, 19.10. HRMS (ESI): calcd for $C_{20}H_{18}O_4$ $[M+H]^+$ 323.12779, found 323.12799.

4.1.8. 2-(3-((4-Bromobenzyl)oxy)benzoyl)-3-hydroxycyclohex-2-en-1-one (a2)

Light yellow solid, Yield: 61%. m.p. 112.1-113.3 °C. ^{1}H NMR (600 MHz, $CDCl_3$) δ 11.87 (s, 1H), 7.60 (d, J=8.4 Hz, 2H), 7.45-7.37 (m, 3H), 7.35 (d, J=7.2 Hz, 1H), 7.31 (s, 1H), 7.23 (d, J=6.6 Hz, 1H), 5.14 (s, 2H), 2.45 (s, 4H), 1.97 (s, 2H). ^{13}C NMR (150 MHz, $CDCl_3$) δ 198.71, 194.10, 157.85, 139.56, 135.64, 131.68, 129.13, 128.83, 121.92, 121.15, 118.43, 114.11, 113.31, 69.36, 38.02, 32.26, 19.10. HRMS (ESI): calcd for $C_{20}H_{17}BrO_4$ $[M+H]^+$ 401.03830, found 401.03729.

4.1.9. 2-(3-((4-Chlorobenzyl)oxy)benzoyl)-3-hydroxycyclohex-2-en-1-one (a3)

Light yellow solid, Yield: 67%. m.p. 111.2-112.4 °C. ^{1}H NMR (400 MHz, $CDCl_3$) δ 16.79 (s, 1H), 7.36 (s, 4H), 7.31 (t, J=8.2 Hz, 1H), 7.09 (dd, J=7.8, 3.6 Hz, 3H), 5.04 (s, 2H), 2.75 (t, J=6.0 Hz, 2H), 2.49 (t, J=6.6 Hz, 2H), 2.12-2.03 (m, 2H). ^{13}C NMR (150 MHz, $CDCl_3$) δ 198.71, 195.90, 194.15, 157.86, 139.56, 135.12, 133.77, 128.84, 128.73, 121.14, 118.43, 114.11, 113.30, 69.33, 38.01, 32.23, 19.09. HRMS (ESI): calcd for $C_{20}H_{17}ClO_4$ $[M+H^+]$ 357.08881, found 357.08857.

4.1.10. 2-(3-((4-Fluorobenzyl)oxy)benzoyl)-3-hydroxycyclohex-2-en-1-one (a4)

Light yellow solid, Yield: 68%. m.p. 84.6-85.7 °C. ^{1}H NMR (600 MHz, $CDCl_3$) δ 7.40 (dd, J=8.4, 5.4 Hz, 2H), 7.30 (t, J=7.8 Hz, 1H), 7.12-7.05 (m, 4H), 5.02 (s, 2H), 2.74 (t, J=6.0 Hz, 2H), 2.54-2.44 (m, 2H), 2.07 (dt, J=13.2, 6.6 Hz, 2H). ^{13}C NMR (150 MHz, $CDCl_3$) δ 198.74, 195.90, 194.14, 163.29, 161.66, 158.06, 139.55, 132.37, 129.48, 129.42, 128.81, 121.09, 118.43, 115.55, 115.40, 114.09, 113.31, 69.43, 38.02, 32.24, 19.09. HRMS (ESI): calcd for $C_{20}H_{17}FO_4$ $[M+H]^+$ 341.11836, found 341.11783

4.1.11. 2-(3-((3-Fluorobenzyl)oxy)benzoyl)-3-hydroxycyclohex-2-en-1-one (a5)

Light yellow solid, Yield: 65%. m.p. 79.8-81.4 °C. ^{1}H NMR (600 MHz, DMSO-d_6) δ 7.47-7.42 (m, 1H), 7.42-7.38 (m, 1H), 7.36 (d, J=7.2 Hz, 1H), 7.31 (d, J=9.0 Hz, 3H), 7.25 (d, J=7.2 Hz, 1H), 7.17 (t, J=7.8 Hz, 1H), 5.18 (s, 2H), 2.46 (s, 4H), 1.98 (dd, J=11.3, 5.3 Hz, 2H). ^{13}C NMR (150 MHz, $CDCl_3$) δ 198.69, 195.86, 194.07, 163.70, 162.07, 157.83, 139.57, 139.19, 130.15, 130.09, 128.84, 122.80, 121.18, 118.41, 114.93, 114.78, 114.34, 114.19, 114.13, 69.28, 38.02, 32.24, 19.10. HRMS (ESI): calcd for $C_{20}H_{17}FO_4$ $[M+H]^+$ 341.11836, found 341.11805.

4.1.12. 3-Hydroxy-2-(3-((4-methylbenzyl) oxy)benzoyl)cyclohex-2-en-1-one (a6)

Light yellow solid, Yield: 65%. m.p. 83.6-84.8 °C; ^{1}H NMR (400 MHz, $CDCl_3$) δ 16.72 (s, 1H), 7.32-7.27 (m, 2H), 7.26 (d, J=7.8 Hz, 1H), 7.17 (d, J=7.8 Hz, 2H), 7.11-7.04 (m, 3H), 5.00 (s, 2H), 2.73 (s, 2H), 2.48 (s, 2H), 2.35 (s, 3H), 2.10-2.01 (m, 2H). ^{13}C NMR (150 MHz, $CDCl_3$) δ 198.71, 195.69, 194.02, 158.20, 139.36, 137.74, 133.44, 129.17, 128.66, 127.66, 120.79, 118.37, 114.06, 69.94, 37.82, 32.13, 21.12, 19.01. HRMS (ESI): calcd for $C_{21}H_{20}O_4$ $[M+H]^+$ 337.14344, found 337.14309.

4.1.13. 2-(3-((2,4-Dichlorobenzyl)oxy)benzoyl)-3-hydroxycyclohex-2-en-1-one (a7)

Light yellow solid, Yield: 69%. m.p. 119.6-121.1 °C. ^{1}H NMR (600 MHz, $CDCl_3$) δ 7.50 (d, J=8.2 Hz, 1H), 7.42 (d, J=1.8 Hz, 1H), 7.32 (t, J=7.8 Hz, 1H), 7.28 (dd, J=8.4, 1.8 Hz, 1H), 7.11 (t, J=7.8 Hz, 3H), 5.14 (s, 2H), 2.75 (t, J=6.0 Hz, 2H), 2.54-2.45 (m, 2H), 2.11-2.03 (m, 2H). ^{13}C NMR (150 MHz,

$CDCl_3$) δ 198.65, 195.93, 194.10, 157.65, 139.64, 134.11, 133.06, 133.03, 129.67, 129.13, 128.90, 127.32, 121.34, 118.35, 114.18, 113.30, 66.64, 38.01, 32.25, 19.10. HRMS (ESI): calcd for $C_{20}H_{16}Cl_2O_4$ $[M+H]^+$ 391.04984, found 391.04933.

4.1.14. 2-(3-((2-Fluorobenzyl)oxy)benzoyl)-3-hydroxycyclohex-2-en-1-one (a8)

Light yellow solid, Yield: 63%. m.p. 64.4-65.9 °C. ^{1}H NMR (600 MHz, $CDCl_3$) δ 7.51 (s, 1H), 7.31 (t, J=7.8 Hz, 2H), 7.17 (s, 1H), 7.15 (s, 1H), 7.11 (dd, J=15.0, 8.4 Hz, 3H), 5.15 (s, 2H), 2.74 (s, 2H), 2.49 (s, 2H), 2.11-2.04 (m, 2H). ^{13}C NMR (150 MHz, $CDCl_3$) δ 198.71, 195.84, 194.10, 161.18, 159.54, 157.86, 139.54, 129.69, 129.64, 128.83, 124.28, 123.72, 121.14, 118.39, 115.37, 115.23, 114.12, 113.34, 103.83, 63.73, 38.01, 32.25, 19.10. HRMS (ESI): calcd for $C_{20}H_{17}FO_4$ $[M+H]^+$ 341.11836, found 341.11758.

4.1.15. 2-(3-((4-Bromo-2-fluorobenzyl)oxy)benzoyl)-3-hydroxycyclohex-2-en-1-one (a9)

Light yellow solid, Yield: 68%. m.p. 87.6-88.5 °C. ^{1}H NMR (400 MHz, $CDCl_3$) δ 16.79 (s, 1H), 7.40 (t, J=7.8 Hz, 1H), 7.35-7.26 (m, 3H), 7.11 (dd, J=7.2, 5.4 Hz, 3H), 5.09 (s, 2H), 2.75 (s, 2H), 2.49 (s, 2H), 2.12-2.03 (m, 2H). ^{13}C NMR (150 MHz, $CDCl_3$) δ 198.64, 195.90, 194.05, 160.84, 159.17, 157.69, 139.63, 130.79, 130.76, 128.87, 127.66, 127.64, 123.13, 123.04, 122.08, 121.32, 119.06, 118.90, 118.33, 114.07, 113.28, 63.26, 63.24, 38.01, 32.25, 19.09. HRMS (ESI): calcd for $C_{20}H_{16}BrO_4$ $[M+H]^+$ 419.02888, found 419.02825.

4.1.16. 2-(3-((4-Chloro-2-fluorobenzyl)oxy)benzoyl)-3-hydroxycyclohex-2-en-1-one (a10)

Light yellow solid, Yield: 65%. m.p. 81.0-81.9 °C. ^{1}H NMR (400 MHz, $CDCl_3$) δ 16.79 (s, 1H), 7.45 (t, J=8.0 Hz, 1H), 7.32 (t, J=8.0 Hz, 1H), 7.17 (d, J=8.4 Hz, 1H), 7.15-7.11 (m, 3H), 7.09 (s, 1H), 5.10 (s, 2H), 2.75 (s, 2H), 2.50 (s, 2H), 2.13-2.02 (m, 2H). ^{13}C NMR (150 MHz, $CDCl_3$) δ 198.65, 195.90, 194.04, 160.87, 159.21, 157.71, 139.63, 134.68, 134.61, 130.51, 130.48, 128.86, 124.73, 124.71,

122.60, 122.51, 121.31, 118.33, 116.22, 116.06, 114.06, 113.31, 63.23, 63.20, 38.02, 32.25, 19.10. HRMS (ESI): calcd for $C_{20}H_{16}ClFO_4$ $[M+H]^+$ 375.07939, found 375.07910.

4.1.17. 2-(3-((4-Bromo-2-fluorobenzyl)oxy)benzoyl)-3-hydroxy-5-methylcyclohex-2-en-1-one (b11)

Light yellow solid, Yield: 63%. m.p. 82.0-83.4 °C. ^{1}H NMR (400 MHz, $CDCl_3$) δ 16.79 (s, 1H), 7.39 (t, J=7.6 Hz, 1H), 7.35-7.27 (m, 3H), 7.10 (s, 3H), 5.08 (s, 2H), 2.79 (d, J=17.6 Hz, 1H), 2.57 (d, J=16.2 Hz, 1H), 2.46 (dd, J=17.8, 10.6 Hz, 1H), 2.33 (dd, J=10.6, 4.2 Hz, 1H), 2.19 (dd, J=16.2, 11.4 Hz, 1H), 1.14 (d, J=6.4 Hz, 3H). ^{13}C NMR (100 MHz, $CDCl_3$) δ 198.54, 195.52, 194.10, 161.34, 158.84, 157.77, 139.66, 130.87, 128.96, 127.76, 123.26, 122.24, 121.38, 119.19, 118.95, 118.41, 114.14, 112.92, 63.36, 63.32, 46.41, 40.22, 26.74, 20.86. HRMS (ESI): calcd for $C_{21}H_{18}BrFO_4$ $[M+H]^+$ 433.04453, found 443.04517.

4.1.18. 2-(3-((4-Bromobenzyl)oxy)benzoyl)-3-hydroxy-5,5-dimethylcyclohex-2-en-1-one (b12)

Light yellow solid, Yield: 65%. m.p. 89.8-90.6 °C. ^{1}H NMR (600 MHz, $CDCl_3$) δ 7.51 (d, J=8.4 Hz, 2H), 7.30 (d, J=8.0 Hz, 3H), 7.07 (d, J=7.8 Hz, 3H), 5.01 (s, 2H), 2.63 (s, 2H), 2.37 (s, 2H), 1.14 (s, 6H). ^{13}C NMR (150 MHz, $CDCl_3$) δ 197.86, 195.13, 193.90, 157.82, 139.32, 135.56, 131.57, 129.03, 128.72, 121.79, 121.01, 118.27, 113.95, 112.21, 69.20, 51.98, 45.79, 30.92, 28.08. HRMS (ESI): calcd for $C_{22}H_{21}BrO_4$ $[M+H]^+$429.06960, found 429.06931.

4.1.19. 2-(3-((4-Bromobenzyl)oxy)benzoyl)-3-hydroxy-5-methylcyclohex-2-en-1-one (b13)

Light yellow solid, Yield: 66%. m.p. 86.0-87.0 °C. ^{1}H NMR (600 MHz, $CDCl_3$) δ 7.51 (d, J=8.4 Hz, 2H), 7.31 (d, J=8.4 Hz, 3H), 7.09 (s, 3H), 5.02 (s, 2H), 2.79 (d, J=16.8 Hz, 1H), 2.57 (d, J=15.0 Hz, 1H), 2.49-2.42 (m, 1H), 2.33 (s, 1H), 2.19 (d, J=16.8 Hz, 1H), 1.14 (d, J=6.6 Hz, 3H). ^{13}C NMR (150 MHz, $CDCl_3$) δ 198.50, 195.42, 194.07, 157.83, 139.50, 135.66, 131.67, 129.12, 128.82, 121.90,

121.12, 118.43, 114.10, 112.83, 69.34, 46.31, 40.13, 26.66, 20.78. HRMS (ESI): calcd for $C_{21}H_{19}BrO_4$ $[M+H]^+$ 415.05395, found 415.05316.

4.1.20. 2-(3-((4-Bromobenzyl)oxy)-2-methylbenzoyl)-3-hydroxycyclohex-2-en-1-one (c14)

Light yellow solid, Yield: 61%. m.p. 108.7-109.9 °C. ^{1}H NMR (400 MHz, $CDCl_3$) δ 17.70 (s, 1H), 7.51 (d, J=7.8 Hz, 2H), 7.32 (d, J=7.8 Hz, 2H), 7.18 (t, J=7.8 Hz, 1H), 6.91 (d, J=8.0 Hz, 1H), 6.73 (d, J=7.4 Hz, 1H), 5.03 (s, 2H), 2.78 (t, J=5.8 Hz, 2H), 2.49-2.38 (m, 2H), 2.15 (s, 3H), 2.09-1.99 (m, 2H). ^{13}C NMR (150 MHz, $CDCl_3$) δ 199.99, 198.33, 193.55, 156.31, 140.41, 136.07, 131.59, 128.79, 126.28, 123.20, 121.62, 118.03, 114.03, 112.28, 69.26, 38.04, 33.05, 19.05, 12.90. HRMS (ESI): calcd for $C_{21}H_{19}BrO_4$ $[M+H]^+$ 415.05395, found 415.05289.

4.1.21. 2-(3-((4-Chlorobenzyl)oxy)-2-methylbenzoyl)-3-hydroxycyclohex-2-en-1-one (c15)

Light yellow solid, Yield: 58%. m.p. 112.3-113.0 °C. ^{1}H NMR (400 MHz, $CDCl_3$) δ 17.70 (s, 1H), 7.37 (d, J=1.8 Hz, 4H), 7.18 (t, J=7.8 Hz, 1H), 6.91 (d, J=8.2 Hz, 1H), 6.73 (d, J=7.6 Hz, 1H), 5.05 (s, 2H), 2.78 (t, J=6.4 Hz, 2H), 2.44 (t, J=6.4 Hz, 2H), 2.15 (s, 3H), 2.04 (m, J=6.4 Hz, 2H). ^{13}C NMR (150 MHz, $CDCl_3$) δ 199.99, 198.31, 193.52, 156.33, 140.41, 135.65, 133.48, 128.65, 128.48, 126.28, 123.21, 118.02, 114.03, 112.29, 69.24, 38.06, 33.06, 19.06, 12.90. HRMS (ESI): calcd for $C_{21}H_{19}ClO_4$ $[M+H]^+$ 371.10446, found 371.10428.

4.1.22. 3-Hydroxy-2-(2-methyl-3-((4-methylbenzyl)oxy)benzoyl)cyclohex-2-en-1-one (c16)

Yield, 61% ; light yellow solid ; m.p. 110.1-110.8 °C ; 1H NMR (600 MHz, $CDCl_3$) δ 7.33 (d, J=6.4 Hz, 2H), 7.18 (dd, J=15.8, 7.4 Hz, 3H), 6.95 (d, J=8.0 Hz, 1H), 6.71 (d, J=7.4 Hz, 1H), 5.04 (s, 2H), 2.77 (s, 2H), 2.44 (s, 2H), 2.37 (s, 3H), 2.15 (s, 3H), 2.04 (s, 2H). ^{13}C NMR (150 MHz, $CDCl_3$) δ 200.08, 198.28, 193.50, 156.67, 140.24, 137.48, 134.13, 129.14, 127.29, 126.21, 123.23, 117.76,

112.35, 103.83, 69.94, 38.07, 33.09, 21.20, 19.06, 12.93. HRMS (ESI): calcd for $C_{22}H_{22}O_4$ [M+H]+ 351.15909, found 351.15887.

4.1.23. 2-(3-((4-Fluorobenzyl)oxy)-2-methylbenzoyl)-3-hydroxycyclohex-2-en-1-one (c17)

Light yellow solid, Yield: 57%. m.p. 112.1-113.0 °C. ^{1}H NMR (400 MHz, $CDCl_3$) δ 17.71 (s, 1H), 7.41 (dd, J=8.0, 5.6 Hz, 2H), 7.19 (t, J=7.8 Hz, 1H), 7.08 (t, J=8.4 Hz, 2H), 6.93 (d, J=8.0 Hz, 1H), 6.73 (d, J=7.4 Hz, 1H), 5.04 (s, 2H), 2.78 (t, J=6.0 Hz, 2H), 2.45 (s, 2H), 2.15 (s, 3H), 2.05 (s, 2H). ^{13}C NMR (150 MHz, $CDCl_3$) δ 200.02, 193.52, 163.14, 161.50, 156.42, 140.38, 132.90, 132.88, 129.00, 128.94, 126.27, 123.22, 117.87, 115.44, 115.30, 114.07, 112.32, 103.83, 69.36, 38.05, 33.04, 19.05, 12.90. HRMS (ESI): calcd for $C_{21}H_{19}FO_4$ $[M+H]^+$ 355.13401, found 355.13342.

4.1.24. 2-(3-((3-Bromobenzyl)oxy)-2-methylbenzoyl)-3-hydroxycyclohex-2-en-1-one (c18)

Light yellow solid, Yield: 62%. m.p. 107.1-107.8 °C. ^{1}H NMR (400 MHz, $CDCl_3$) δ 17.71 (s, 1H), 7.60 (s, 1H), 7.46 (d, J=7.8 Hz, 1H), 7.37 (d, J=7.6 Hz, 1H), 7.28 (s, 1H), 7.24 (s, 1H), 7.19 (t, J=7.8 Hz, 1H), 6.91 (d, J=7.8 Hz, 1H), 6.74 (d, J=7.6 Hz, 1H), 5.05 (s, 2H), 2.79 (t, J=6.4 Hz, 2H), 2.45 (t, J=6.4 Hz, 2H), 2.17 (s, 3H), 2.09-2.01 (m, 2H). ^{13}C NMR (150 MHz, $CDCl_3$) δ 199.97, 198.28, 193.52, 156.28, 140.43, 139.49, 130.83, 130.09, 130.02, 126.30, 125.58, 123.25, 122.54, 118.01, 112.29, 69.13, 38.05, 33.05, 19.06, 12.92. HRMS (ESI): calcd for $C_{21}H_{19}BrO_4$ $[M+H]^+$ 415.05395, found 415.05364.

4.1.25. 2-(3-((4-Chloro-2-fluorobenzyl)oxy)-2-methylbenzoyl)-3-hydroxycyclohex-2-en-1-one (c19)

Light yellow solid, Yield: 52%. m.p. 102.8-104.0 °C. ^{1}H NMR (400 MHz, $CDCl_3$) δ 17.74 (s, 1H), 7.52 (t, J=8.0 Hz, 1H), 7.25 (d, J=7.8 Hz, 1H), 7.22 (d, J=7.8 Hz, 1H), 7.18 (d, J=9.6 Hz, 1H), 6.99 (d, J=8.0 Hz, 1H), 6.79 (d, J=7.4 Hz, 1H), 5.16 (s, 2H), 2.83 (t, J=6.0 Hz, 2H), 2.49 (t, J=6.2 Hz, 2H), 2.20 (s, 3H), 2.14-2.05 (m, 2H). ^{13}C NMR (150 MHz, $CDCl_3$) δ 199.95, 198.32, 193.56, 160.75, 159.08,

156.09, 140.46, 134.28, 130.07, 126.34, 124.66, 124.64, 123.28, 118.27, 116.04, 115.98, 112.28, 63.33, 63.31, 38.04, 33.05, 19.05, 12.86. HRMS (ESI): calcd for $C_{21}H_{18}ClFO_4$ $[M+H]^+$ 389.09504, found 389.09498.

4.1.26. 2-(3-((4-Chloro-2-fluorobenzyl)oxy)-2-methylbenzoyl)-3-hydroxy-5-methylcyclo-hex-2-en-1-one (c20)

Light yellow solid, Yield: 59%. m.p. 106.4-107.2 °C. ^{1}H NMR (400 MHz, $CDCl_3$) δ 17.74 (s, 1H), 7.44 (t, J=8.0 Hz, 1H), 7.24 (m, J=15.2, 8.8 Hz, 3H), 7.01 (d, J=8.2 Hz, 1H), 6.80 (d, J=7.6 Hz, 1H), 5.17 (s, 2H), 2.88 (dd, J=18.0, 2.4 Hz, 1H), 2.56 (dd, J=18.8, 11.0 Hz, 2H), 2.37 (s, 1H), 2.21 (s, 3H), 1.19 (d, J=6.4 Hz, 3H). ^{13}C NMR (150 MHz, $CDCl_3$) δ 199.63, 197.77, 193.45, 160.74, 159.08, 156.07, 140.39, 134.28, 130.02, 126.35, 124.66, 123.27, 123.12, 123.03, 118.25, 116.04, 115.97, 112.28, 46.35, 40.90, 40.88, 26.53, 20.84, 12.84. HRMS (ESI): calcd for $C_{22}H_{20}ClFO_4$ $[M+H]^+$ 403.11069, found 403.11021.

4.1.27. 2-(3-(Benzyloxy)-4-chloro-2-methylbenzoyl)-3-hydroxycyclohex-2-en-1-one (c21)

Light yellow oil, **Yield**: 47%. ^{1}H NMR (600 MHz, $CDCl_3$) δ 7.45 (d, J=6.0 Hz, 2H), 7.43 (t, J=7.2 Hz, 2H), 7.31 (d, J=8.4 Hz, 1H), 6.86 (d, J=6.0 Hz, 1H), 5.00 (s, 2H), 2.80 (t, J=6.6 Hz, 2H), 2.47 (t, J=6.6 Hz, 2H), 2.20 (d, J=3.0 Hz, 3H), 2.07 (t, J=6.0 Hz, 2H). ^{13}C NMR (100 MHz, $CDCl_3$) δ 199.00, 198.37, 193.69, 153.15, 139.54, 136.95, 130.44, 129.60, 128.56, 128.22, 128.03, 127.62, 122.29, 114.00, 74.58, 38.05, 32.97, 19.09, 13.57. HRMS (ESI): calcd for $C_{21}H_{19}ClO_4$ $[M+Na]^+$ 393.08641 found 393.08688.

4.1.28. 2-(4-Chloro-3-((4-fluorobenzyl)oxy)-2-methylbenzoyl)-3-hydroxycyclohex-2-en-1-one (c22)

Light yellow solid, Yield: 51%. m.p. 87.6-88.9 °C. ^{1}H NMR (600 MHz, $CDCl_3$) δ 7.42-7.48 (m, 2H), 7.30 (d, J=9.0 Hz, 1H), 7.10 (t, J=8.4 Hz, 2H), 6.85 (d, J=8.4 Hz, 1H), 4.95 (s, 2H), 2.80 (t, J=6.0 Hz,

2H), 2.46 (t, J=9.0 Hz, 2H), 2.16 (s, 3H), 2.07 (p, J=6.0 Hz, 2H). ^{13}C NMR (100 MHz, $CDCl_3$) δ 198.94, 198.35, 193.62, 163.93, 161.48, 152.92, 139.58, 132.72, 130.35, 130.14, 130.06, 129.50, 127.66, 122.32, 115.54, 115.33, 113.98, 73.87, 38.07, 32.96, 19.09, 13.56. HRMS (ESI): calcd for $C_{21}H_{18}ClFO_4$ $[M+Na]^+$ 411.07699 found 411.07910.

4.1.29. 2-(3-((4-Bromobenzyl)oxy)-2-nitrobenzoyl)-3-hydroxycyclohex-2-en-1-one (d23)

Light yellow solid, Yield: 60%. m.p. 154.5-155.4 °C. ^{1}H NMR (400 MHz, $CDCl_3$) δ 16.47 (s, 1H), 7.41 (t, J=9.0 Hz, 3H), 7.33 (d, J=8.0 Hz, 2H), 7.13 (d, J=7.8 Hz, 1H), 6.86 (d, J=6.8 Hz, 1H), 5.17 (s, 2H), 2.77 (t, J=6.0 Hz, 2H), 2.43 (t, J=6.2 Hz, 2H), 2.05 (p, J=6.0 Hz, 2H). ^{13}C NMR (100 MHz, $CDCl_3$) δ 196.31, 193.83, 150.98, 137.76, 137.13, 134.41, 132.74, 131.88, 128.72, 122.26, 119.05, 115.69, 113.02, 70.65, 37.60, 31.95, 19.12. HRMS (ESI): calcd for $C_{20}H_{16}BrNO_6$ $[M+Na]^+$ 468.00532 found 468.00683.

4.1.30. 3-Hydroxy-2-(3-((4-methylbenzyl)oxy)-2-nitrobenzoyl)cyclohex-2-en-1-one (d24)

Light yellow solid, Yield: 53%. m.p. 142.4-143.8 °C. ^{1}H NMR (600 MHz, $CDCl_3$) δ 7.46 (t, J=7.8 Hz, 1H), 7.33 (d, J=6.0 Hz, 2H), 7.19 (d, J=7.8 Hz, 2H), 7.16 (d, J=6.0 Hz, 1H), 6.83 (d, J=7.8 Hz, 1H), 5.19 (s, 2H), 2.76 (t, J=6.6 Hz, 2H), 2.43 (t, J=6.0 Hz, 2H), 2.35 (s, 3H), 2.04 (m, J=6.6 Hz, 2H). ^{13}C NMR (100 MHz, $CDCl_3$) δ 196.41, 196.34, 193.88, 151.33, 138.02, 137.79, 136.93, 132.62, 132.37, 129.42, 127.23, 118.71, 115.90, 113.06, 71.42, 37.62, 31.97, 21.27, 19.13. HRMS (ESI): calcd for $C_{21}H_{19}NO_6$ $[M+Na]^+$ 404.11046 found 404.11040.

4.1.31. 2-(3-(1-(4-Fluorophenyl)ethoxy)-2-nitrobenzoyl)-3-hydroxycyclohex-2-en-1-one (d25)

Light yellow solid, Yield: 63%. m.p. 166.4-167.4 °C. ^{1}H NMR (400 MHz, $CDCl_3$) δ 16.53 (s, 1H), 7.45-7.39 (m, 2H), 7.36 (t, J=8.0 Hz, 1H), 7.09 (t, J=8.6 Hz, 2H), 6.95 (d, J=8.4 Hz, 1H), 6.81 (d, J=7.6 Hz, 1H), 5.46 (d, J=6.4 Hz, 1H), 2.81 (t, J=8.0 Hz, 2H), 2.47 (t, J=6.0 Hz, 2H), 2.08 (p, J=6.4 Hz, 2H), 1.69 (d, J=6.4 Hz, 3H). ^{13}C NMR (100 MHz, $CDCl_3$) δ 196.40, 196.35, 193.86, 163.57,

161.12, 150.29, 137.40, 136.70, 132.17, 127.35, 127.27, 118.63, 116.97, 115.98, 115.76, 113.05, 37.61, 31.98, 24.39, 19.11. HRMS (ESI): calcd for $C_{21}H_{18}FNO_6$ $[M+Na]^+$ 422.10104 found 422.10142.

4.1.32. 3-Hydroxy-2-(3-((4-isopropylbenzyl)oxy)-2-nitrobenzoyl)cyclohex-2-en-1-one (d26)

Light yellow solid, Yield, 58% ; ; m.p. 116.5-117.8°C ; 1H NMR (600 MHz, $CDCl_3$) δ 7.47 (t, J=9.0 Hz, 1H), 7.37 (d, J=7.8 Hz, 2H), 7.26 (s, 2H), 7.18 (d, J=8.4 Hz, 1H), 6.84 (d, J=7.8 Hz, 1H), 5.19 (s, 2H), 2.94-2.89 (m, 1H), 2.77 (t, J=6.0 Hz, 2H), 2.43 (t, J=6.6 Hz, 2H), 2.04 (p, J=6.6 Hz, 2H), 1.25 (d, J=6.0 Hz, 6H). ^{13}C NMR (100 MHz, $CDCl_3$) δ 196.41, 196.30, 193.84, 151.38, 149.10, 136.94, 132.73, 132.62, 127.33, 126.82, 118.70, 115.87, 113.07, 77.43, 77.11, 76.79, 71.44, 37.62, 33.93, 31.97, 24.02, 19.14. HRMS (ESI): calcd for $C_{23}H_{23}NO_6$ $[M+Na]^+$ 432.14176 found 432,14119.

4.1.33. 2-(3-((3,5-Dimethylbenzyl)oxy)-2-nitrobenzoyl)-3-hydroxycyclohex-2-en-1-one (d27)

Light yellow solid, Yield: 52%. m.p. 153.4-154.9 °C. ^1H NMR (400 MHz, $CDCl_3$) δ 16.50 (s, 1H), 7.46 (t, J=8.0 Hz, 1H), 7.15 (d, J=8.4 Hz, 1H), 7.05 (s, 2H), 6.96 (s, 1H), 6.83 (d, J=7.6 Hz, 1H), 5.15 (s, 2H), 2.76 (t, J=6.0 Hz, 2H), 2.43 (t, J=6.4 Hz, 2H), 2.33 (s, 6H), 2.04 (m, J=6.2 Hz, 2H). ^{13}C NMR (100 MHz, $CDCl_3$) δ 196.45, 196.27, 193.80, 151.47, 138.36, 137.79, 136.97, 135.31, 132.65, 129.98, 124.95, 118.71, 115.97, 113.06, 71.69, 37.64, 31.98, 21.37, 19.15. HRMS (ESI): calcd for $C_{22}H_{21}NO_6$ $[M+Na]^+$ 418.02611 found 418.02616.

4.1.34. 3-Hydroxy-5-methyl-2-(3-((4-methylbenzyl)oxy)-2-nitrobenzoyl)cyclohex-2-en-1-one (d28)

Light yellow solid, Yield: 49%. m.p. 112.3-113.6 °C. ^1H NMR (400 MHz, $CDCl_3$) δ 16.46 (s, 1H), 7.46 (t, J=8.0 Hz, 1H), 7.32 (d, J=7.6 Hz, 2H), 7.17 (t, J=10.0 Hz, 3H), 6.82 (d, J=7.6 Hz, 1H), 5.18 (s, 2H), 2.85-2.71 (m, 1H), 2.49 (t, J=12.0 Hz, 2H), 2.35 (s, 4H), 2.14 (dd, J=12.0, 8.0 Hz, 1H), 1.11 (d,

J=8.0 Hz, 3H). ^{13}C NMR (100 MHz, $CDCl_3$) δ 196.21, 195.73, 193.80, 151.32, 138.00, 136.88, 132.63, 132.38, 129.42, 127.23, 118.73, 115.91, 71.42, 45.80, 39.68, 26.71, 21.28, 20.81. HRMS (ESI): calcd for $C_{22}H_{21}NO_6$ $[M+Na]^+$ 418.02666 found 418.02582.

4.1.35. 2-(3-((4-Bromo-2-fluorobenzyl)oxy)-2-nitrobenzoyl)-3-hydroxycyclohex-2-en-1-one (d29)

Light yellow solid, Yield: 60%. m.p. 158.0-159.8 °C. ^{1}H NMR (400 MHz, $CDCl_3$) δ 16.46 (s, 1H), 7.42 (t, J=6.8 Hz, 1H), 7.40-7.46 (m, 1H), 7.35 (m, J=8.0, 1H), 7.31-7.27 (m, 1H), 7.19 (d, J=8.4 Hz, 1H), 6.88 (d, J=7.6 Hz, 1H), 5.23 (s, 2H), 2.78 (t, J=6.0 Hz, 2H), 2.43 (t, J=6.0 Hz, 2H), 2.05 (m, J=6.0, Hz, 2H). ^{13}C NMR (100 MHz, $CDCl_3$) δ 196.32, 196.24, 193.86, 160.89, 158.39, 150.79, 137.28, 132.90, 130.47, 130.42, 128.07, 128.04, 119.31, 119.10, 118.86, 115.56, 113.00, 64.74, 37.60, 31.96, 19.13. HRMS (ESI): calcd for $C_{20}H_{15}BrFNO_6$ $[M+Na]^+$ 485.99590 found 485.99506.

4.1.36. 2-(3-((4-Bromo-2-fluorobenzyl)oxy)-2-nitrobenzoyl)-3-hydroxy-5-methylcyclohex-2-en-1-one (d30)

Light yellow solid, Yield: 63%. m.p. 140.9-142.8 °C. ^{1}H NMR (400 MHz, $CDCl_3$) δ 16.45 (s, 1H), 7.43 (dt, J=16.0, 8.0 Hz, 2H), 7.37 (d, J=8.2 Hz, 1H), 7.32 (s, 1H), 7.22 (d, J=8.4 Hz, 1H), 6.91 (d, J=8.0 Hz, 1H), 5.26 (s, 2H), 2.83 (dd, J=16.0, 4.0 Hz, 1H), 2.52 (dd, J=16.0, 12.0 Hz, 2H), 2.19 (d, J=10.2 Hz, 1H), 1.60 (s, 1H), 1.15 (d, J=4.0 Hz, 3H). ^{13}C NMR (100 MHz, $CDCl_3$) δ 196.03, 195.72, 193.76, 160.88, 158.39, 150.75, 137.21, 132.90, 130.43, 128.03, 119.32, 119.08, 118.84, 115.55, 112.53, 64.69, 45.77, 39.65, 26.70, 20.79. HRMS (ESI): calcd for $C_{21}H_{17}BrFNO_6$ $[M+Na]^+$ 500.01155 found 500.01368.

4.1.37. 2-(3-((2,4-Dichlorobenzyl)oxy)-2-nitrobenzoyl)-3-hydroxycyclohex-2-en-1-one (d31)

Light yellow solid, Yield: 55%. m.p. 150.4-152.1 °C. ^{1}H NMR (400 MHz, $CDCl_3$) δ 16.48 (s, 1H), 7.62 (d, J=8.4 Hz, 1H), 7.43 (t, J=8.0 Hz, 1H), 7.42 (d, J=2.0 Hz, 1H), 7.32 (d, J=8.0, 1H), 7.19 (d, J=8.0 Hz, 1H), 6.89 (d, J=8.0 Hz, 1H), 5.27 (s, 2H), 2.78 (t, J=6.0 Hz, 2H), 2.43 (t, J=6.0 Hz, 2H), 2.05

(m, J=6.0 Hz, 2H). ^{13}C NMR (100 MHz, $CDCl_3$) δ 196.30, 196.27, 193.86, 150.80, 137.39, 134.46, 133.00, 132.41, 131.86, 129.38, 129.11, 127.72, 119.28, 115.51, 112.99, 67.89, 37.61, 31.96, 19.14. HRMS (ESI): calcd for $C_{20}H_{15}Cl_2NO_6$ $[M+Na]^+$ 458.01686 found 458.01734.

4.1.38. 2-(3-((2,4-Dichlorobenzyl)oxy)-2-nitrobenzoyl)-3-hydroxy-5-methylcyclohex-2-en-1-one (d32)

Light yellow solid, Yield: 51%. m.p. 114.5-116.2 °C. ^{1}H NMR (400 MHz, $CDCl_3$) δ 16.47 (s, 1H), 7.65 (d, J=8.0 Hz, 1H), 7.47 (t, J=8.0 Hz, 1H), 7.45 (s , 1H), 7.35 (dd, J=8.0, 1H), 7.22 (d, J=8.4 Hz, 1H), 6.92 (d, J=7.6 Hz, 1H), 5.30 (s, 2H), 2.84 (dd, J=16.0, 4.0 Hz, 1H), 2.58-2.48 (m, 2H), 2.33 (dt, J=8.0, 6.0 Hz, 1H), 2.18 (dd, J=16.0, 12.0 Hz, 1H), 1.15 (d, J=6.4 Hz, 3H). ^{13}C NMR (100 MHz, $CDCl_3$) δ 196.06, 150.77, 137.61, 137.37, 134.45, 133.02, 132.40, 131.87, 129.37, 129.10, 127.72, 119.31, 115.51, 112.54, 67.88, 26.72, 20.82. HRMS (ESI): calcd for $C_{21}H_{17}Cl_2NO_6$ $[M+Na]^+$ 472.03251 found 472.03186.

4.1.39. 2-(3-((2,4-Difluorobenzyl)oxy)-2-nitrobenzoyl)-3-hydroxycyclohex-2-en-1-one (d33)

Light yellow solid, Yield: 57%. m.p. 130.7-132.5 °C. ^{1}H NMR (400 MHz, $CDCl_3$) δ 16.47 (s, 1H), 7.48 (t, J=8.0 Hz, 1H), 7.42 (t, J=7.8 Hz, 1H), 7.21 (d, J=8.4 Hz, 1H), 6.94 (t, J=8.0 Hz, 1H), 6.88 (d, J =4.0 Hz, 1H), 6.84 (d, J=8.6 Hz, 1H), 5.24 (s, 2H), 2.77 (s, 2H), 2.43 (s, 2H), 2.05 (t, J=6.0 Hz, 2H). ^{13}C NMR (100 MHz, $CDCl_3$) δ 196.25, 164.24, 161.45, 150.86, 137.78, 137.19, 132.84, 132.52, 130.65, 119.24, 115.66, 113.00, 111.98, 111.76, 104.08, 103.83, 103.58, 64.75, 38.86, 35.01, 19.11. HRMS (ESI): calcd for $C_{20}H_{15}F_2NO_6$ $[M+Na]^+$ 426.07596 found 426.07518.

4.2. Bioassay

Human HPPD (*h*HPPD) and human homogentisate 1,2-dioxygenase (*h*HGD) were required to determine the inhibitory activity using the coupled enzyme reaction. Starting from cDNA, pET-28a-*h*HPPD and pET-28a-*h*HGD plasmids were constructed as previously described [22,23] to express the

aforesaid enzymes. The recombinant enzymes were over-expressed in *E. coli* BL21 cells (DE3) for which cells were incubated at 37 °C in Luria broth media containing appropriate antibiotics. When the E. coli growth reached an A_{600} of ~0.6, the temperature was decreased to 20 °C, and the cells were then grown for additional 14 h (*h*HPPD) and 40h (*h*HGD). The cells were collected by centrifugation (8000g, 5 min), and washed twice with (150 mM NaCl, 20 mM HEPES, pH 7.0) before disruption by sonication. The mixture was then centrifuged at 13500g for 45 min to get the crude enzyme. The crude supernatant containing recombinant enzyme was then loaded onto Ni-NTA column (Invitrogen) equilibrated with 150 mM NaCl and 20 mM HEPES, pH 7.0, and enzyme was purified with imidazole gradient and eluted with 250 mM imidazole. The overexpression and the relative molecular weight of recombinant HPPDs were validated by sodium dodecyl sulfate polyacrylamide gel electrophoresis (SDS-PAGE), while the purity was estimated using ImageJ software (ImageJ 1.52a, Bethesda, MD, USA). As HGD is highly active compared with HPPD, the crude enzyme was directly used for in vitro inhibitory activity of synthetic compounds against *h*HPPD. Indeed, the inhibitory activity was evaluated by monitoring the formation of maleylacetoacetate at 318 nm in 96-well plates at 30 °C using a UV/visible plate reader (Biotech, Winooski, VT, USA). The volume of the reaction mixture was 200 μL containing 50 μM HPPA, 2 mM sodium ascorbate, 20 mM HEPES buffer (pH 7.0), 100 μM FeSO4, and appropriate amounts of HGD and HPPD. To ensure that the reaction was efficiently coupled, the amount of HGD was set to be in large excess compared with HPPD by setting the rate constant *k* at 0.1 and 0.01, respectively. The reaction components were equilibrated at 30 °C for about 10 min before the measurement, whereas the inhibitors were dissolved in dimethyl sulfoxide (DMSO) and diluted with testing buffer before use. Fitted curve and IC_{50} values were obtained using OriginPro 7.5 software (OriginLab, Northampton, MA).

4.3. Computational method

Since no ligand-bound human HPPD crystal structure is available, the homology modeling was used to construct a structure, which keeps the ligand-bound conformations of residues at the active site. The HPPD crystal structure derived from rat HPPD (PDB ID: 1SQI) was selected as template and human HPPD protein sequence (NCBI GI: 258588704) as template. Of note, human and rat HPPDs share a sequence identity of 90%. The SWISS-MODEL tool [24] was used for homology modeling. Then, the constructed human HPPD three-dimensional structure was dealt with Discovery Studio 4.0 to add missing hydrogens. For the docking simulation, the chemical structures of the inhibitors were prepared by SYBYL 7.0 followed by the 2,000 steepest descent for minimization and 2,000 conjugate gradient minimizations. The GOLD 3.0 was used to dock the constructed inhibitors into human HPPD active site whose radius was set to 10 Å by using a genetic algorithm (GA) with 100 runs, and Co (II) as a chelate center. The semiempirical score function [25] offered by Autodock 4 was used to assess the binding free energy between inhibitors and constructed human HPPD.

Supporting Information

Detailed analytical data of representative intermediates and target compounds.

Acknowledgment

We are grateful for the financial support from the National Key Research and Development Program of China (No. 2017YFA0505200) and the National Natural Science Foundation of China (No. 21837001 and 21672079); Hubei Province Natural Science Foundation (No. 2018CFA072); the self-determined research funds of Central China Normal University (CCNU18ZDPY01 and CCNU18TS007) from the colleges' basic research and operation of MOE".

References

[1] G.R. Moran, 4-Hydroxyphenylpyruvate dioxygenase, Arch. Biochem. Biophys. 433 (2005) 117-

128.

[2] M. Gunsior, J. Ravel, G.L. Challis, C.A. Townsend, Engineering *p*-hydroxyphenylpyruvate dioxygenase to a p-hydroxymandelate synthase and evidence for the proposed benzene oxide intermediate in homogentisate formation, Biochemistry. 43 (2004) 663-674.

[3] B. Lindblad, G. Lindstedt, S. Lindstedt, The mechanism of enzymic formation of homogentisate from *p*-hydroxyphenylpyruvate, J. Am. Chem. Soc. 92 (1970) 7446-7449.

[4] G. Morrow, R.M. Tanguay, Biochemical and clinical aspects of hereditary tyrosinemia type 1, in: Hered. Tyrosinemia, Springer, 2017: pp. 9-21.

[5] E. Natt, K. Kida, M. Odievre, M. Di Rocco, G. Scherer, Point mutations in the tyrosine aminotransferase gene in tyrosinemia type II., Proc. Natl. Acad. Sci. 89 (1992) 9297-9301.

[6] K. Tomoeda, H. Awata, T. Matsuura, I. Matsuda, E. Ploechl, T. Milovac, A. Boneh, C.R. Scott, D.M. Danks, F. Endo, Mutations in the 4-hydroxyphenylpyruvic acid dioxygenase gene are responsible for tyrosinemia type III and hawkinsinuria, Mol. Genet. Metab. 71 (2000) 506-510.

[7] J.M. Brownlee, B. Heinz, J. Bates, G.R. Moran, Product analysis and inhibition studies of a causative asn to ser variant of 4-hydroxyphenylpyruvate dioxygenase suggest a simple route to the treatment of Hawkinsinuria, Biochemistry. 49 (2010) 7218-7226.

[8] U. Rüetschi, R. Cerone, C. Pérez-Cerda, M.C. Schiaffino, S. Standing, M. Ugarte, E. Holme, Mutations in the 4-hydroxyphenylpyruvate dioxygenase gene (HPD) in patients with tyrosinemia type III, Hum. Genet. 106 (2000) 654-662.

[9] A.J. Preston, C.M. Keenan, H. Sutherland, P.J. Wilson, B. Wlodarski, A.M. Taylor, D.P. Williams, L.R. Ranganath, J.A. Gallagher, J.C. Jarvis, Ochronotic osteoarthropathy in a mouse model of alkaptonuria, and its inhibition by nitisinone, Ann. Rheum. Dis. 73 (2014) 284-289.

[10] G.R. Moran, 4-Hydroxyphenylpyruvate dioxygenase and hydroxymandelate synthase: Exemplars of the α-keto acid dependent oxygenases, Arch. Biochem. Biophys. 544 (2014) 58-

68.

[11] J. Larochelle, F. Alvarez, J.-F. Bussières, I. Chevalier, L. Dallaire, J. Dubois, F. Faucher, D. Fenyves, P. Goodyer, A. Grenier, others, Effect of nitisinone (NTBC) treatment on the clinical course of hepatorenal tyrosinemia in Quebec, Mol. Genet. Metab. 107 (2012) 49-54.

[12] D.C. Bartlett, C. Lloyd, P.J. McKiernan, P.N. Newsome, Early nitisinone treatment reduces the need for liver transplantation in children with tyrosinaemia type 1 and improves post-transplant renal function, J. Inherit. Metab. Dis. 37 (2014) 745-752.

[13] C.M. Keenan, A.J. Preston, H. Sutherland, P.J. Wilson, E.E. Psarelli, T.F. Cox, L.R. Ranganath, J.C. Jarvis, J.A. Gallagher, Nitisinone arrests but does not reverse ochronosis in alkaptonuric mice, in: JIMD Rep., 2015: pp. 45-50.

[14] N. Mohan, P. McKiernan, D.A. Kelly, M.A. Preece, A. Green, J. Buckels, A.D. Mayer, Indications and outcome of liver transplantation in tyrosinaemia type 1, Eur. J. Pediatr. 158 (1999) S049--S054.

[15] W.G. van Ginkel, R. Jahja, S.C.J. Huijbregts, A. Daly, A. MacDonald, C. De Laet, D. Cassiman, F. Eyskens, I.M.L.W. Körver-Keularts, P.J. Goyens, others, Neurocognitive outcome in tyrosinemia type 1 patients compared to healthy controls, Orphanet J. Rare Dis. 11 (2016) 87.

[16] E.A. Lock, P. Gaskin, M.K. Ellis, W. Mclean Provan, M. Robinson, L.L. Smith, M.P. Prisbylla, L.C. Mutter, Tissue Distribution of 2-(2-Nitro-4-trifluoromethylbenzoyl)cyclohexane- 1,3-dione (NTBC): Effect on Enzymes Involved in Tyrosine Catabolism and Relevance to Ocular Toxicity in the Rat, Toxicol. Appl. Pharmacol. 141 (1996) 439-447.

[17] A. Śledź Paweł and Caflisch, Protein structure-based drug design: From docking to molecular dynamics, Curr. Opin. Struct. Biol. 48 (2018) 93-102.

[18] A. van Almsick, New HPPD-inhibitors--a proven mode of action as a new hope to solve current weed problems, Outlooks Pest Manag. 20 (2009) 27-30.

[19] Y.L. Xu, H.Y. Lin, R.J. Cao, Z.Z. Ming, W.C. Yang, G.F. Yang, Pyrazolone-quinazolone hybrids: A novel class of human 4-hydroxyphenylpyruvate dioxygenase inhibitors, Bioorganic Med. Chem. 22 (2014) 5194-5211.

[20] D.W. Wang, H.Y. Lin, R.J. Cao, T. Chen, F.X. Wu, G.F. Hao, Q. Chen, W.C. Yang, G.F. Yang, Synthesis and herbicidal activity of triketone-quinoline hybrids as novel 4-hydroxyphenylpyruvate dioxygenase inhibitors, J. Agric. Food Chem. 63 (2015) 5587-5596.

[21] J.M. Brownlee, K. Johnson-Winters, D.H.T. Harrison, G.R. Moran, Structure of the ferrous form of (4-hydroxyphenyl)pyruvate dioxygenase from *Streptomyces avermitilis* in complex with the therapeutic herbicide, NTBC, Biochemistry. 43 (2004) 6370-6377.

[22] Y.L. Xu, H.Y. Lin, X. Ruan, S.G. Yang, G.F. Hao, W.C. Yang, G.F. Yang, Synthesis and bioevaluation of pyrazole-benzimidazolone hybrids as novel human 4-Hydroxyphenylpyruvate dioxygenase inhibitors, Eur. J. Med. Chem. 92 (2015) 427-438.

[23] D.W. Wang, H.Y. Lin, B. He, F.X. Wu, T. Chen, Q. Chen, W.C. Yang, G.F. Yang, An efficient one-pot synthesis of 2-(aryloxyacetyl)cyclohexane-1,3-diones as herbicidal 4-hydroxyphenylpyruvate dioxygenase inhibitors, J. Agric. Food Chem. 64 (2016) 8986-8993.

[24] A. Waterhouse, M. Bertoni, S. Bienert, G. Studer, G. Tauriello, R. Gumienny, F.T. Heer, T.A.P. de Beer, C. Rempfer, L. Bordoli, R. Lepore, T. Schwede, SWISS-MODEL: homology modelling of protein structures and complexes., Nucleic Acids Res. (2018) gky427.

[25] R. Huey, G.M. Morris, A.J. Olson, D.S. Goodsell, A semiempirical free energy force field with charge-based desolvation, J. Comput. Chem. 28 (2007) 1145-1152.

Highlights

- A new strategy of hydrophobicity-oriented drug design (HODD) was developed for the design of HPPD inhibitors.
- A series of 2-(3-(benzyloxy)benzoyl)-3-hydroxycyclohex-2-en-1-one analogs with new chemical scaffold were prepared and most of them showed good activity against recombinant human HPPD.
- Compound **d23** was identified as the most potent candidate (IC_{50} = 47 nM), about 2-fold more potent than NTBC (IC_{50} = 85 nM), demonstrating good potential for the treatment of type I tyrosinemia, alkaptunuria and hawkinsinuria